Velocity-optimized diffusion for ultra-fast polymer-based resistive gas sensors

S.-L. Tan, J.A. Covington and J.W. Gardner

Abstract: Conducting polymers are an attractive candidate for use in thin film resistive gas and vapour sensors, but their use has been limited by their apparently slow response times ranging from tens of seconds to minutes. In studying this problem, the authors have discovered that the response time is highly dependent upon the velocity at which the analyte flows across the sensor surface. This type of sensor operates at ambient temperature, and so the authors have attributed this behaviour to the combination of a reduced time for diffusion of the analyte in the carrier gas (pulse broadening) and faster diffusion through a disturbed boundary layer on the polymer surface. A finite element model has been developed to explore this phenomenon. The actual responses of two types of carbon-black/polymer composite resistive sensors have been measured at velocities ranging from 50 to 1500 cm/s to pulses of ethanol and toluene vapour in air, using a purpose-built automated low-volume microchannel flow delivery system. The effect of velocity on the sensors response has been found to vary for different analytes, with a linear velocity coefficient of 1 to 15 s/cm for ethanol and toluene vapour in air, respectively in the diffusion coefficient. The magnitude and rise time of the sensor responses were computed for different velocities and agrees well with the theoretical finite element model. Under optimal conditions, the fastest sensor was found to exhibit a rise time of less than 100 ms, which would be expected to fall even further for thinner films. These results suggest that conducting polymer resistive sensors could be designed to work with a 1 s duty cycle making them attractive for applications where rapid monitoring is required, e.g. on unmanned airborne vehicles and land-based mobile robots.

1 Introduction

The sampling rate has always been an important parameter in any practical application of a sensor. Polymer-based resistive sensors are commonly used in the analysis of vapours due to their ease of fabrication, room temperature operation and wide range of available materials, but this type of gas sensor tends to suffer from a slower response time than others, e.g. metal oxide. The response time of polymer sensors is typically in the range of 10 to 100 s [1–8], which we have previously postulated as being diffusion-rate limited [1].

Another important factor that affects the sensor response time is the actual duration of the injected pulse of the analyte within a carrier gas (i.e. the pulse width). The pulse width defines the length of time for which the polymer film is exposed to the analyte. The impact of this is two-fold; firstly, the volume of analyte required for a test is proportional to the exposure time and hence the amount of material that must be flushed out of the flow system. Secondly, it determines the analysis or sampling time because the signal and data processing can only begin after the complete exposure cycle has occurred. Some recent studies [2, 3] have demonstrated that it is possible to use transient information for improved gas and odour discrimination, but this requires the measurement cycle to be completed in a reasonable time (e.g. less than 30 s).

It should be noted that a poor sensor-chamber design often leads to an unnecessary increase in the exposure duration through a low flow velocity and non-plug flow (e.g. a mixing effect). Here, we define the flow velocity as the average speed or group speed of the test analyte flow across the sensor surface (i.e. the volumetric flow-rate/cross-sectional area). The design of the sensor chamber is an important factor in the behaviour of the entire flow system; this is even more critical when considering arrays of sensors as all of the sensors should be exposed simultaneously, with the same pulse shape for pattern recognition. In most chamber designs, a small inlet and outlet are usually connected to a large-volume chamber for ease of interfacing to a mass flow system (pump and valves) using inter-connecting tubing [4, 5]. Such designs suffer from the requirement of a long injection time to fill the entire chamber and hence they need a large volume of test analyte. In addition, it is possible to have an uneven concentration gradient across the chamber through circulation or turbulence associated with non-laminar flow. Also, the ratio of the cross-sectional area of the inlet/outlet and chamber will result in the velocity across the sensors being reduced by the same ratio. For example, Meckes and Behrens [4] constructed a miniaturised version of a commercial chamber but operated it at a constantly low flow rate. Only small quantities of analytes are required in miniaturised systems, but if they operate at a low flow rate then the sensor response time is compromised.

Liu *et al.* [6] were the first to report the effect of flow rate on gas sensor sensitivity in 1995 [6]. More recently Eklov *et al.* [5] showed that an increase in the flow rate could

IEE Proceedings online no. 20050035

doi:10.1049/ip-smt:20050035

Paper first received 16th June and in final revised form 14th October 2005

The authors are with School of Engineering, University of Warwick, Coventry CV4 7AL, UK

E-mail: j.w.gardner@warwick.ac.uk

improve the response time of their sensor array, but instead chose a lower flow rate for its ability to give a differential response to their type of sensor array. A sensor array with different response profiles was desired in their case due to its ability to provide a larger diversity of responses to improve their pattern recognition algorithm rather than similar responses. Yoshigoe *et al.* [9] simply reported the influence of flow rate on their sensor response, but did not elaborate upon this statement. Briglin and Lewis [10] reported in 2003 fast resistive polymer gas sensors by operating their chamber at flow rates in excess of 5.9 l/min, equivalent to a flow velocity of about 1500 cm/s. A fast sensor response was again reported but they did not investigate the effect of flow rate on the sensor response time.

Traditionally, gas sensor systems are operated with a relatively low flow rate, because it is generally believed that the response time is diffusion-rate limited. Typical velocities across the sensors are anywhere between 20 and 200 cm/s [4–6, 11].

The physiology of the human olfactory system is not yet completely understood, but nevertheless, our understanding has been greatly increased over the past 5 years [12]. It is interesting to note that the flow rates chosen for gas sensors are generally slow when compared to the biological system. The human olfactory system operates at higher flow rates of between 180 and 1100 ml/s, i.e. 300–1540 cm/s across the olfactory epithelium [13–15]. This range of flow rates can be conveniently classified according to three categories: a normal intake of breath, typically 300 cm/s, a medium sniff at 880 cm/s, and a forceful sniff at 1540 cm/s. The duration of the intake of air also varies with the three types of sniff. Studies have shown that, as expected, increasing the sniffing velocity is usually accompanied by a reduced sniffing duration associated with the fixed capacity of the lungs, where the duration of a sniff varies anywhere from 1 to 3 s [13]. Figure 1 shows the range of operation for traditional gas sampling systems, our ultra-fast microchannel system described in detail below, and three biological operations. We believe operating at a higher velocity should result in a more favourable response for gas sensors and hence this study investigates these issues. In addition, we feel that a short pulse width is preferable as it gives an increase in the sampling rate. More significantly, it reduces the volume of analyte required and that in turn leads to a much faster recovery time as the removal of the analyte mass from the chamber and associated tubing is often a key practical concern.

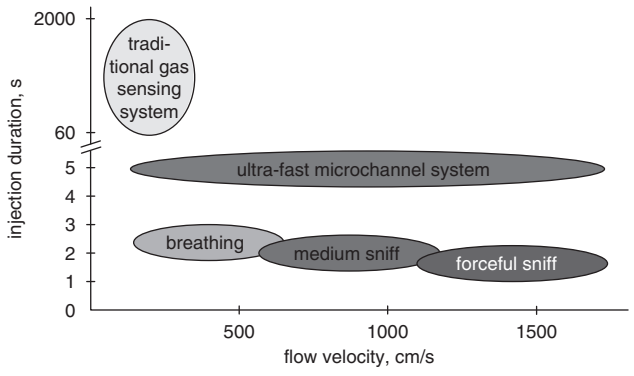

Fig. 1 *Injection duration and flow velocity for a traditional gas sensing system, an ultra-fast microchannel system and the human olfactory system*

2 Sensor fabrication and system design

Figure 2 shows the general design of our ultra-fast sampling system, which houses ten polymer-based resistive gas sensors. The silicon-based substrate for the chemoresistors was fabricated in-house using UV lithography techniques. Each device is 4 × 4 mm in size and consists of a pair of thin gold electrodes on a SiO_2/Si substrate with an electrode length of 1000 μm and an inter-electrode gap of 75 μm. Commercial polymers were mixed together with a 20% carbon-black loading by weight, in a suitable solvent, at room temperature. Two exemplar polymers were used in the tests here, namely commercially available poly-ethylene-co-vinyl acetate (PEVA) and poly-styrene-co-butadiene (PSB). The carbon black material comprises of carbon nanospheres with a diameter of typically 50 – 80 nm. The mixture was first sonicated for 10 min and then airbrush coated using a micro spraying system on to the device through a mechanical micromask. This gave a circular coating typically 1 mm in diameter. The electrical resistance of the polymer sensors was controlled through the deposition process to a value of about 1 kΩ (±30%) and a typical film thickness was about 20 μm (±25%).

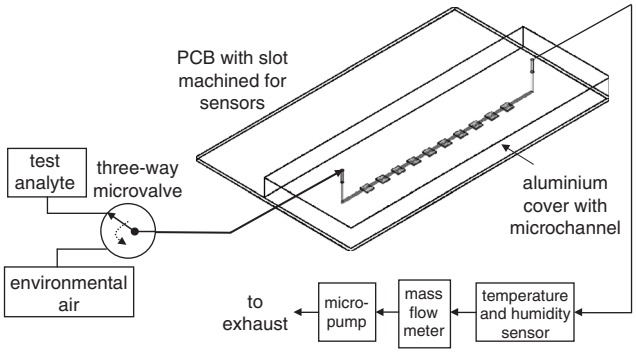

Fig. 2 *Experimental setup*

A schematic of the components of the mass flow system is given in Fig. 2 and consists of a commercial mass flow meter, a relative humidity and temperature sensmitter, an NMP 05 micropump, a three-way microvalve, a digital input/output card, and an in-house designed data acquisition board with dual 16-bit ADCs. The circuit used to measure the sensor resistance is simply an operational amplifier configured in the inverting mode with a reference voltage source at the input, a reference input resistor, and the sensor used as the feedback resistor. The data acquisition board provides multiplexing control for access to the ten sensor channels and the sampling rate is typically 4 ms per sensor. All these units are controlled via custom-designed software written in Labview version 6.1 (National Instruments) on a PC in order to provide fully automated test cycles and data logging for subsequent signal analysis.

The three-way switching microvalve controls the injection duration of the test analyte by selecting between the test analyte and a carrier gas and operates in about 1.5 ms. The carrier gas used in all our experimental work was simply the ambient air in the laboratory without any control of temperature or humidity and so relates closer to real-world applications. The air was delivered to the sensors through a 500 μm × 1000 μm × 100 mm microchannel with the sensors mounted linearly along it. It then flows across the temperature and humidity sensor, through the mass flow meter and finally into the micropump. The flow velocity is set by the operating voltage of the pump and depends upon

the generated pressure. The concentration of the analyte in the headspace was approximately constant throughout all of the experiments although it will vary somewhat because the saturated headspace concentration is a function of ambient temperature.

3 Finite element simulation

It is essential to understand the dynamics of the microfluidic flow since it determines the nature of the analyte delivery to the sensors and their subsequent time-based response. Various studies on chamber designs have considered the location of the sensors for optimal response magnitude, but often neglect the possible effects of non-simultaneous exposure, turbulence and mixing. To avoid such problems, a finite element modelling package was used in which the meshes can be designed to estimate the flow of the gas through the system and across and into the sensors. A geometrical model was created from the physical dimensions of the microchannel. A multi-physics mode, employing the Navier-Stokes (NS) equation, is used to simulate laminar transport and a convection and diffusion (CD) equation is used to simulate the diffusion and dispersion of the injected analyte pulse [15]. The partial differential equations (PDEs) used for the simulations are described as follows:

The NS equation is:

$$\mu\nabla^2 V + \rho(V\cdot\nabla)V + \nabla P = 0 \tag{1}$$

where μ is the viscosity, ρ is the density, P is the pressure and V is the velocity.

The CD equation can be written as:

$$\frac{\partial C}{\partial t} + \nabla\cdot(-D\nabla C + CV) = 0 \tag{2}$$

where D is the diffusion coefficient and C is the analyte concentration.

At the inlet, the analyte concentration is defined as:

$$C = C_{\mathrm{i}} \times (t < t_{\mathrm{PW}}) \tag{3}$$

where C_{i} is the injected concentration of the analyte and t_{PW} is the exposure time.

At the outlet, the convective contribution to the mass transport is assumed to be much larger than the diffusive contribution:

$$(-D\nabla C + C\cdot v)\cdot \boldsymbol{n} = (C\cdot v)\cdot \boldsymbol{n} \tag{4}$$

where $\boldsymbol{n}$ is the normal vector to the respective boundary.

Of great interest is the effect of 'pulsewidth-broadening' of the test analyte pulse over time as it is delivered to the sensors along the linear microchannel. Due to the diffusion and dispersion of the test analyte pulse, while travelling along the microchannel, the fronts of the pulse will broaden out with time. It is important to know the rate of broadening at different velocities, as this will determine the ultimate sensor response. For example, consider the perfect model of a square vapour pulse being presented to the sensor at a flow velocity of 500 cm/s; a basic first-order exponential model of the sensor response generates an expected response as shown in Fig. 3*a*. However, if the velocity is reduced down to 10 cm/s, the delivered pulse will broaden out into a bell-like curve and the magnitude of the response will also be reduced. So a sensor with the same response model will respond very differently as illustrated in Fig. 3*b*. In addition to the response time and magnitude, the pulse is clearly delayed, i.e. there is a time lag between the switch created by the pulse and it reaching the sensor. This problem can be exacerbated by long inlet tubes, a poor chamber design, and a low flow velocity for analyte

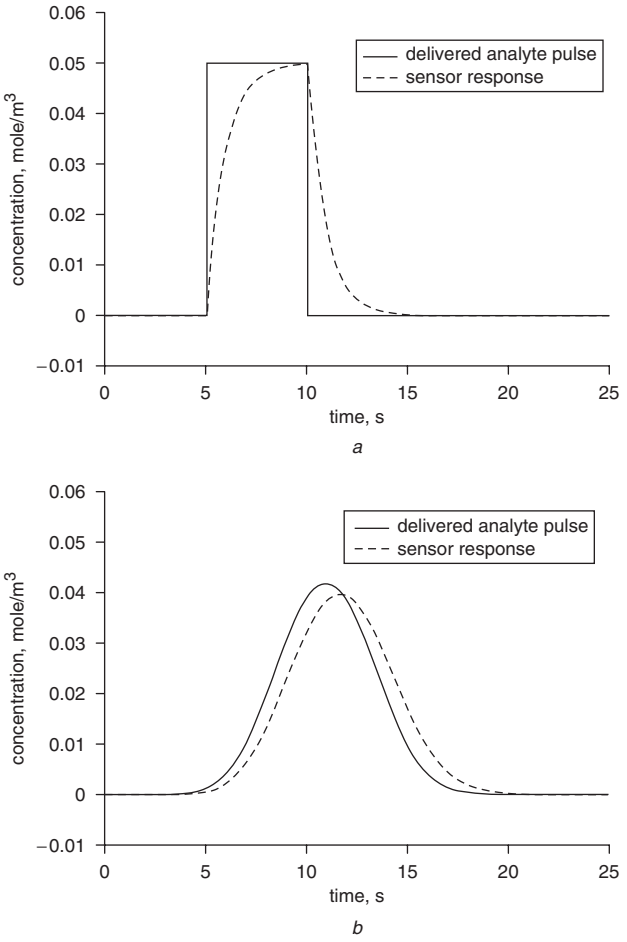

Fig. 3 *Simulation of the pulse delivered to the sensor surface and the actual sensor response*
a For a velocity of 500 cm/s
b For a velocity of 10 cm/s

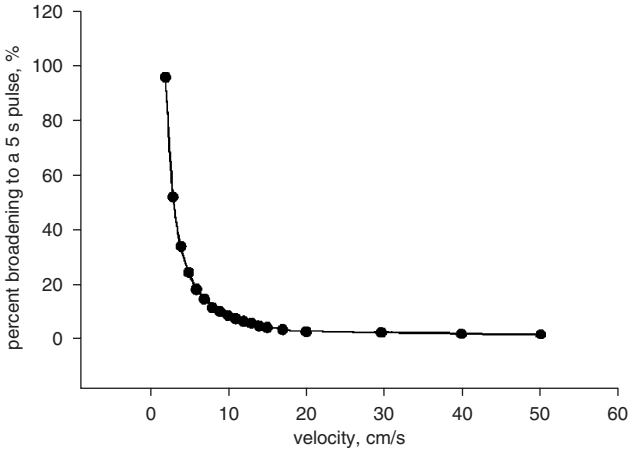

Fig. 4 *Broadening effect of the delivered pulse as function of flow velocity*

is delivery. The amount of broadening at the end of our microchannel was predicted when a 5 s ethanol vapour pulse is injected at different velocities. The simulation results, shown in Fig. 4, demonstrate that significant broadening of the ethanol pulse occurs, in our case, when the flow velocity is below a value of 20 cm/s. At a velocity above 100 cm/s, negligible broadening is observed. Simulations with different test analytes have shown the same basic results with the precise broadening depending upon

the diffusion coefficient of the analyte in the carrier gas (i.e. air).

To study the effect of the velocity on the polymer sensor response, the model was extended to include a 20 μm thick polymer layer at the bottom of the 500 μm (height) microchannel. Figure 5*a* shows a partial finite element mesh of the microchannel with the polymer sensor. The mesh comprises 1143 computational nodes and 1917 elements. The PDEs used are based on the simple reaction-diffusion model as proposed in [16] and [17]. The partition coefficient of the analyte in the polymer was incorporated simply by modifying the boundary conditions. To account for the partition coefficient, c, which is defined by the equilibrium distribution of analyte molecules between the microchannel and the polymer, the boundary conditions were modified as follows (Fig. 5*b*):

$$\left[\frac{\partial C_C}{\partial t} + \nabla(-D\nabla C_C + C_C V)\right] \cdot \boldsymbol{n} = M(C_P - cC_C) \quad \text{at } \partial\Omega_{C,P} \tag{5}$$

$$\left[\frac{\partial C_P}{\partial t} + \nabla(-D\nabla C_P + C_P V)\right] \cdot \boldsymbol{n} = M(cC_C - C_P) \quad \text{at } \partial\Omega_{P,C} \tag{6}$$

where C_P is the concentration of the analyte in the polymer and C_C is the concentration of the analyte in the microchannel (i.e. air). The partition coefficient c can be defined as:

$$c = \frac{C_P}{C_C} \tag{7}$$

Because there will be discontinuities in the concentration profile at the boundaries between the microchannel and polymer, two separate variables, C_C and C_P were used to describe the concentration in the respective phases. In order to obtain a continuous flux over the phase boundaries, a special type of boundary condition, using the stiff-spring method was used. Instead of defining a Dirichlet concentration condition according to the partition coefficient c, which would destroy the continuity of the flux, a continuous flux condition was defined. At the same time, the concentration is forced to the desired values. M is a large number to let the concentration differences in the brackets on the right of (5) and (6) approach zero. Note that these boundary conditions also give us continuity in flux, provided that M is sufficiently large [18].

The effective diffusion coefficient of the polymer was modelled for the sake of simplicity with a linear term as follows:

$$D = D_o(1 + v_o V) \tag{8}$$

where v_o is a first-order velocity coefficient and D_o is the diffusion coefficient at zero velocity.

In theory, the effective diffusion coefficient will be related to the size of the analyte molecules, the molar mass and the porosity of the sensing material which can be derived using the Fuller-Schettler-Giddings and Stokes-Einstein equations [19]. This is expected to be analyte-polymer specific. Here, the aim is to investigate the impact of flow velocity on the response of the polymer-based sensors, hence a linear term was used for simplicity.

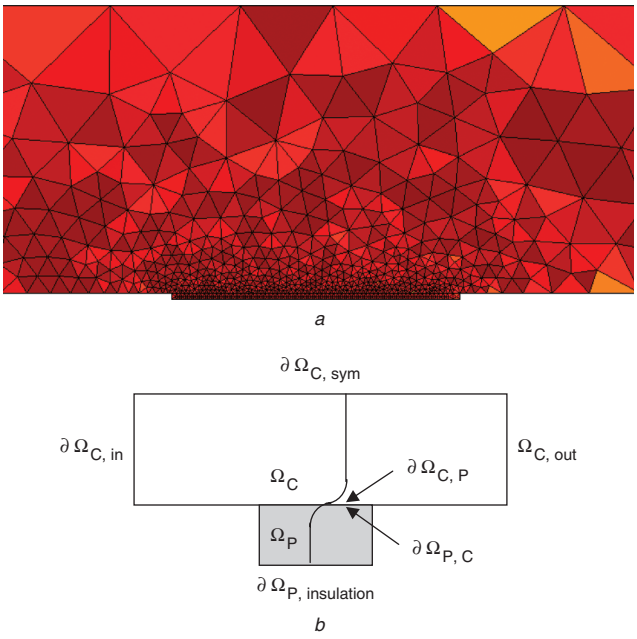

Fig. 5
a Geometrical mesh model for the FE simulation of the sensor response
b The boundary conditions used in the simulation

4 Effect of velocity

The two most important parameters in defining the response kinetics are the pulse width and the velocity. It has been shown in [1–8] that the pulse width ranges from 60 s to in excess of 2000 s. As we wish to create a fast response system that requires low volumes of test analyte, the pulse width should be reduced to a minimum. Various pulse widths have been investigated ranging from 100 ms to 10 s. This range was selected based on the expected response times of our sensors and an interesting analogy to the sniffing duration of the human olfactory system. The tests showed that with a narrow pulse width, the velocity has to be increased before any detectable response of the sensor can be observed. Thus the need to reduce the pulse width may result in the practical need for ultra-fast high precision microvalves and data acquisition system.

Our investigations have shown that the flow velocity directly affects the response magnitude ($\Delta V/V$) and rise time. Again, the range of velocities tested relate to the human sniffing rate. We have also investigated the effect of analyte injection direction (swapping inlet with outlet) and sensor placement. As predicted from our simulations, at low velocities the sensor responses are time-shifted and broadening occurs towards the end of the microchannel. Swapping the inlet and outlet simply affects the sensors towards the end of the microchannel, but there is no effect when operating at higher flow velocities. Similar observations were made when the sensors are re-ordered. In fact, the sensors placement architecture can be used to determine the flow direction, and at low values, determine the flow velocity based on the time-shifting and their physical separation.

4.1 Baseline resistance

The baseline resistance is defined as the value of the resistance of the sensor prior to any exposure to an analyte. In order to determine the impact of velocity on the sensor response, the baselines have to be measured under different velocities to ensure that the shift in response is not solely a result of the shift in the baseline. The baseline voltage of each sensor (equivalent resistance) was monitored with increasing velocity. The variation in sensor baseline resistance (up to 30%) is the difference in resistance across

different sensors, hence it will not contribute to any measurement error since the baseline voltage was measured for each individual sensor. Figure 6 shows the baseline voltage against velocity plot for PEVA and PSB sensors. It was found that they varied less than 0.2% ($\Delta V/V$). This may be due to the cooling effect as the velocity is increased, but it is insignificant compared to the response magnitude that could be up to 40%.

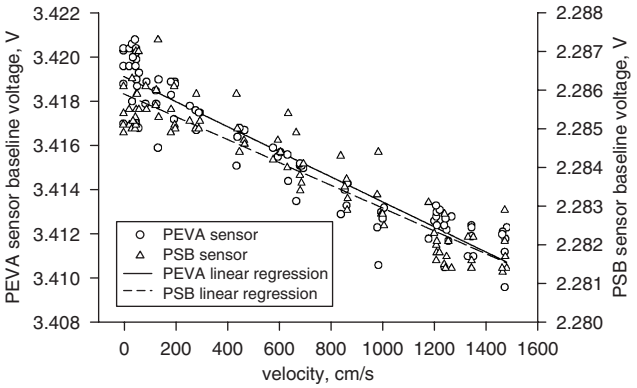

Fig. 6 *Observed effect of the flow velocity on the baseline voltage (proportional to resistance) for two different polymer sensors*

4.2 Typical responses to ethanol and toluene vapour in air

All of our experiments were performed at the same nominal concentrations of ethanol and toluene vapours in air. The decision not to have environmental control on the temperature and humidity of the air was made to simplify the system and work under conditions closer to real-world situations. In practice the measurements were conducted within a time frame of 1 h and so the measurement conditions were similar, with the temperature throughout all experiments being around 30°C (±2°C) and the relative humidity around 40% (±5%). Figures 7 and 8 show the typical normalised responses of a PEVA sensor to a 5 s ethanol or toluene vapour pulse in air at different velocities, respectively. The carrier gas was allowed to flow through the system for 1 min before each experiment began to stabilise the resistance and micropump flow. The vapour pulse was then turned on at time, $t = 1$ s and turned off at time, $t = 6$ s giving a 5 s pulse duration. Similar measurements were conducted at increasing velocities. Figures 9

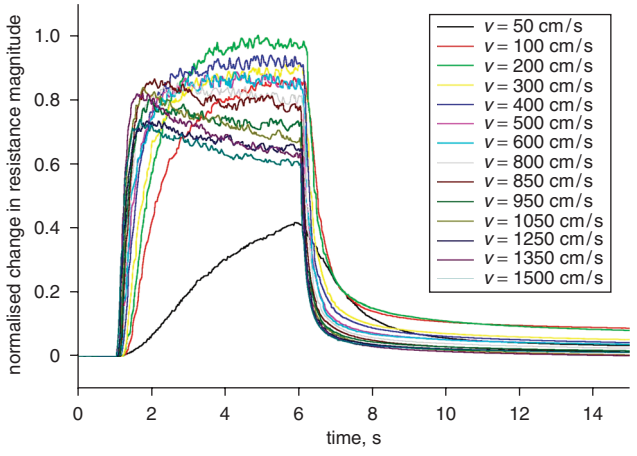

Fig. 7 *Normalised PEVA sensor response to a pulse of ethanol vapour in air at different velocities*

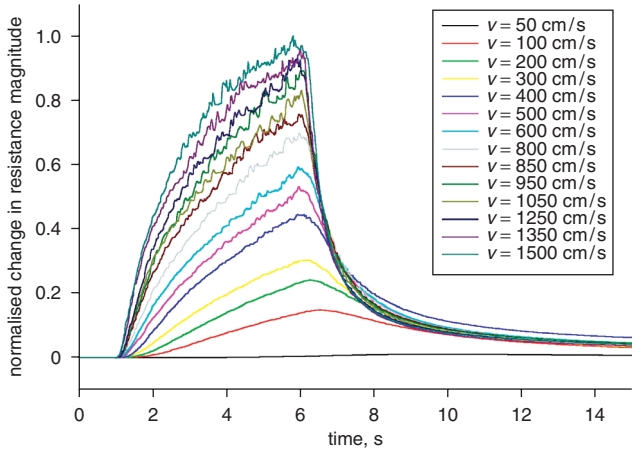

Fig. 8 *Normalised PEVA sensor response to pulse of toluene vapour in air at different velocities*

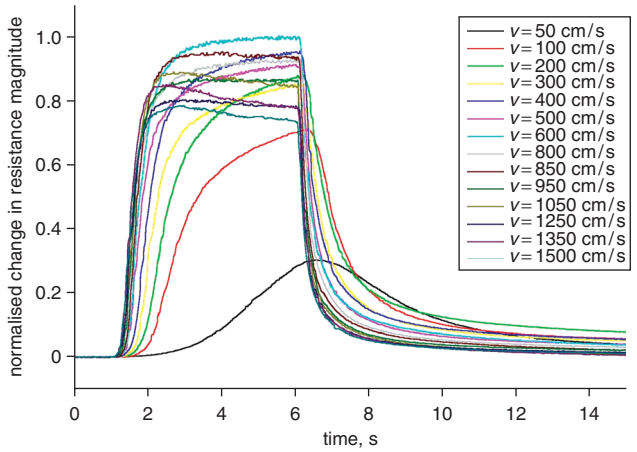

Fig. 9 *Normalised PSB sensor response to pulse of ethanol vapour in air at different velocities*

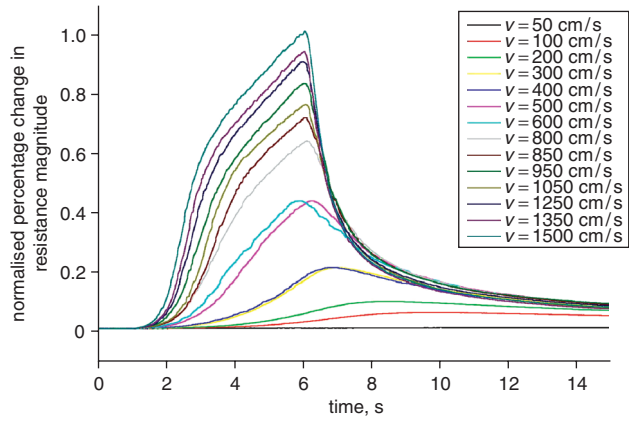

Fig. 10 *Normalised PSB sensor response to a pulse of toluene vapour in air at different velocities*

and 10 show the typical normalised responses of a PSB sensor to a 5 s ethanol or toluene vapour pulse in air at different velocities, respectively. It was also observed that the response profiles of the sensors at higher flow velocities (> 500 cm/s) appeared to be noiser, especially for PEVA sensors responding to both the ethanol and toluene vapours. Although the simulation results for the microchannel did not report any abnormality (i.e. laminar flow), we believe that some undesirable flow complication (such as mixing and turbulent effects) could well be being

contributed by other subsystems such as the mass flow system. These include the interconnecting tubings of various sizes and other monitoring devices (mass flow sensors, temperature and humidity sensor) of varying cross-sections that could contribute to alter the steady-state concentration of the test analyte. The extent of variation is also sensing material specific, resulting in greater impact on PEVA sensor as oppose to PSB sensor.

4.3 Maximum response magnitude

Figures 11 and 12 show the normalised maximum response magnitude of the sensors to either the ethanol on the toluene vapours in air at the different velocities. The $\Delta V_{max}/\Delta V$ of the responses were used in all plots. In the case of ethanol vapour, as the velocity is gradually increased, the response magnitude increased to a maximum at a velocity of approximately 200 cm/s and subsequently it slightly reduced. We attribute this effect to the competition of the polar ethanol vapour with water (humidity). For the toluene vapour, this effect is not observed and hence the response magnitude increased linearly with velocity. It is important to note that the increase in response magnitude is not a result of any increase in delivered toluene vapour concentration, but a result of an increase in response time. This will approach the saturation limit if the exposure duration is increased even at lower velocities.

The temperature effect on the sensor response magnitude was studied from 30°C to 50°C. Our investigations showed that when the temperature was increased, the response magnitude decreased. The rate of decrease within the tested range is approximately 0.7%/°C (although not linear throughout the entire operating range [1]) and as expected when considering the processes governed by the partition coefficient it is inversely related to the absolute temperature.

4.4 Rise time

Figures 13 and 14 show the effect of velocity on the growth coefficient (i.e. rise time) of the sensors. It is well known that polymer sensors used in chemical detection can be approximated by a first-order exponential response model [16, 17]. Using this exponential model the sensor resistance can be expressed in terms of the rise time as shown in (9):

$$R = R_0(1 - e^{-t/\tau_0}) \tag{9}$$

where R_0 is the base resistance and τ_0 is the rise time (which is related to the RC time constant).

This approach has been used to compare the response times of different polymer sensors in [16] and [17]. Clearly, the response (rise) time decreases as the velocity is increased, showing that the sensor responds faster with increasing velocity for both types of sensors to ethanol and toluene vapour in air. The extent of the velocity impact on the diffusion coefficient differs for the ethanol and toluene vapours in air. For the ethanol vapour the velocity coefficient given by (8) is one, whereas for the toluene vapour it is approximately 15. This is possibly related to the

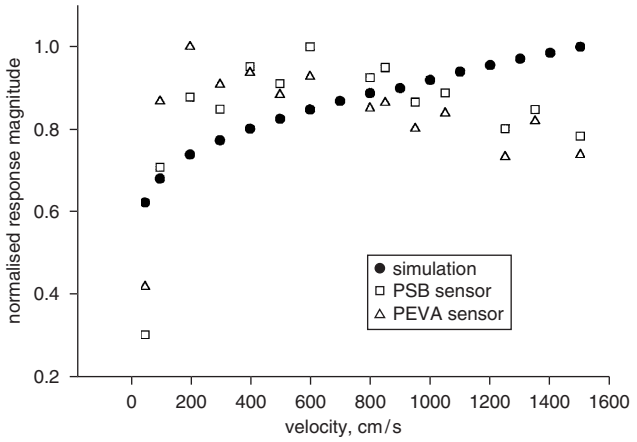

Fig. 11 *Normalised experimental and theoretical the response magnitudes of two polymer sensors to a pulse of ethanol vapour in air at different velocities*

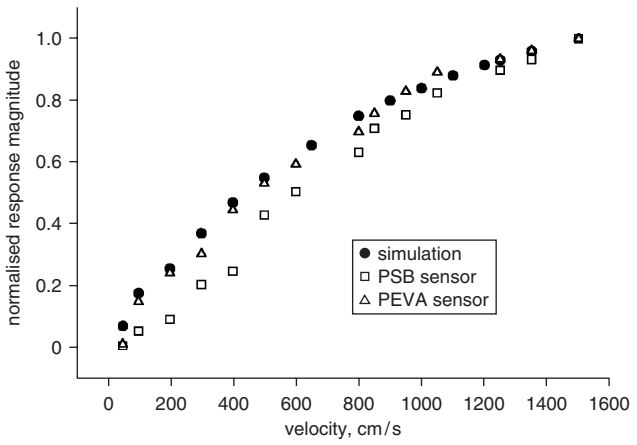

Fig. 12 *Normalised experimental and theoretical response magnitudes to a pulse of toluene vapour in air at different velocities*

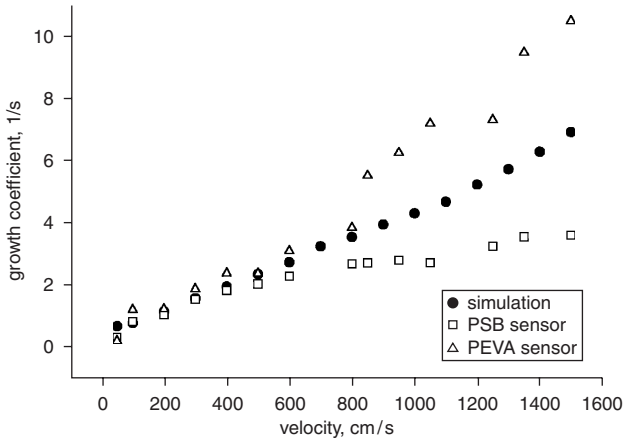

Fig. 13 *Observed and theoretical growth coefficient of the two polymer sensors to pulse of ethanol vapour in air at different velocities*

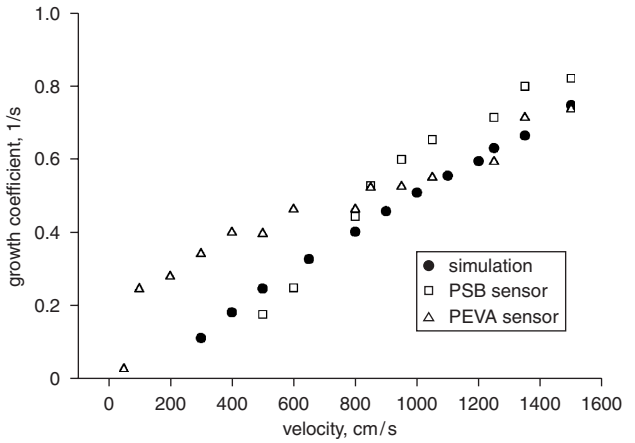

Fig. 14 *Observed and theoretical growth coefficient of the two polymer sensors to pulse of toluene vapour in air at different velocities*

size of the analyte molecule and the porosity of the polymer sensing layer. The fastest responding sensor has a rise time of only 95 ms and hence, it is ultra-fast as compared to the typical response time of similar polymer-based sensors which are in the range of seconds to minutes.

The temperature affects the rise time positively as opposed to the response magnitude. As the temperature is increased, the rise time decreases, giving a faster responding sensor. The average improvement is approximately 10 ms/°C. This can be understood from the basic Arrhenius diffusion equation.

$$D = D_{\hat{0}} \exp\left(\frac{-Q}{R\mathrm{T}}\right) \tag{10}$$

where Q is the activation energy, T is the absolute temperature and R is the gas constant.

Since the diffusion coefficient is a strong function of temperature, any increase in the temperature results in a large increase in the diffusion coefficient and hence the decrease in rise time, although it will also increase the pulse-broadening effect described earlier.

5 Conclusions

We have reported on a technique to improve the response time and relative magnitude of polymer-based gas sensors by increasing the velocity of the carrier gas and reducing the length of the injected pulse. We attribute the improvements in response time and magnitude to an increase in the effective diffusion coefficient of the analyte into a thin polymer sensing film. We have also demonstrated that the use of a microchannel delivery system removes some undesirable effects associated with larger chambers. The finite element model provides an easy and convenient technique to estimate the response of these sensors. We believe that the use of a microchamber design together with the selection of an optimal operating velocity and pulse width are important in the design of better hand-held gas sensor systems and e-noses. It is also interesting to note that the thickness of our polymer films is comparable to the thickness of the olfactory epithelium in the human olfactory system and that the optimal flow velocity is again comparable to that occurring during a normal sniff. Perhaps the human olfactory system has already evolved to overcome the dynamical problem of pulse-broadening?

6 References

1 Covington, J.A., Gardner, J.W., Briand, D., and de Rooij, N.F.: 'A polymer-gate FET sensor array for detecting organic vapours', *Sens. Actuators B, Chem.*, 2001, **77**

2 Wilson, D.M., and DeWeerth, S.P.: 'Odour discrimination using steady-state and transient characteristics of tin-oxide sensors', *Sens. Actuators B, Chem.*, 1995, **28**, pp. 123–128

3 Gutierrez-Osuna, R.H.T., and Schiffman, N.S.S.: 'Transient response analysis of an electronic nose using multi-exponential models', *Sens. Actuators B, Chem.*, 1999, **61**, pp. 170–182

4 Meckes, A., and Behrens, J.: 'Microfluidic system for the integration and cyclic operation of gas sensors', *Sens. Actuators*, 1999, **76**, pp. 478–483

5 Eklov, T., and Lundstrom, I.: 'Gas mixture analysis using a distributed chemical sensor system', *Sens. Actuators B Chem.*, 1999, **57**, pp. 274–282

6 Liu, S.-J., Shen, H.-X., and Feng, J.-X.: 'Effects of gas flow-rates on a Clark-type oxygen gas sensor', *Anal. Chim. Acta Comput. Tech. Optim.*, 1995, **313**, pp. 89–92

7 Sotzing, G.A., Phend, J.N., Grubbs, R.H., and Lewis, N.S.: 'Highly sensitive detection and discrimination of biogenic amines utilizing arrays of polyaniline/carbon black composite vapour detectors', *Chem. Mater.*, 2000, **12**, pp. 593–595

8 Matzger, A.J., Lawrence, C.E., Brubbs, R.H., and Lewis, N.S.: 'Combinatorial approaches to the synthesis of vapour detector arrays for use in an electronic nose', *J. Comb. Chem.*, 2000, **2**, pp. 301–304

9 Yoshigoe, T., Nishina, T., Sato, S., Yamaki, K., and Endo, M.: 'Development of gas sensors for volatile organic compounds by using solid polymer electrolyte membrane electrodes', *Anal. Sci.*, 2001, **17**, pp. 1023–1025

10 Briglin, S.W., and Lewis, N.S.: 'Characterization of the temporal response profile of carbon black – polymer composite detectors to volatile organic vapours', *J. Phys. Chem. B*, 2003, **107**, pp. 11031–11042

11 Nieuwenhuizen, M. S., and Harteveld, J. L.N.: 'An automated SAW gas sensor testing system', *Sens. Actuators A, Phys.*, 1994, pp. 219–229

12 Pearce, T.C., Schiffman, S.S., Nagle, H.T., and Gardner, J.W.: 'Handbook of Machine Olfaction: Electronic Nose Technology' (Wiley-VCH, Weinheim, 2002)

13 Sobel, S., Khan, R.M., Hartley, C.A., Sullivan, E.V., and Gabrieli, J.D.E.: 'Sniffing longer rather than stronger to maintain olfactory detection threshold', *Chem. Senses*, 2000, **25**, pp. 1–8

14 Hahn, I., Scherer, P.W., and Mozell, M.M.: 'Velocity profiles measured for airflow through a large-scale model of the human nasal cavity', *J. Appl. Physiol.*, 1993, **75**, pp. 2273–2287

15 Keyhani, K., Scherer, P.W., and Mozell, M.M.: 'A numerical model of nasal odorant transport for the analysis of human olfaction', *J. Theor. Biol.*, 1997, **186**, pp. 1–2

16 Matsunaga, N., Sakai, G., Shimanoe, K., and Yamazoe, N.: 'Formulation of gas dynamics for thin film semiconductor gas sensor based on simple reaction-diffusion equation', *Sens. Actuators B, Chem.*, 2003

17 Gardner, J.W., Bartlett, P.N., and Pratt, K.F.E.: 'Modelling of gas-sensitive conducting polymer device', *IEE Proc., Circuits, Devices Syst.*, 1995, **142**

18 Fontes, E., Byrne, P., Sundqvist, J., Bosander, P., and Marklund, M.: 'FEMLAB Chemical Engineering user manual (version 2.1), Comsol, Inc., March 2001

19 Cussler, E.L.: 'Diffusion: Mass Transfer in Fluid Systems' (Cambridge University Press, New York, 1984)